Dong *et al. Skeletal Muscle* (2024) 14:29
https://doi.org/10.1186/s13395-024-00363-1

Skeletal Muscle

RESEARCH Open Access

Role and mechanism of myonectin in severe acute pancreatitis: a crosstalk between skeletal muscle and pancreas

Xiaowu Dong[1†], Weiwei Luo[1†], Yaodong Wang[2†], Qingtian Zhu[1], Chenchen Yuan[1], Weiming Xiao[1], Weijuan Gong[1], Guotao Lu[1,3*], Xiaolei Shi[1*] and Jin Li[4*]

Abstract

Background Severe acute pancreatitis (SAP) is characterized by high mortality rates and various complications, including skeletal muscle atrophy, which significantly exacerbates its outcomes. Despite its clinical relevance, the mechanistic understanding of the relationship between skeletal muscle and the pancreas in SAP remains limited. Our study aimed to elucidate this "organ crosstalk" and its potential implications.

Methods We established an SAP mouse model through pancreatic duct ligation (PDL) and evaluated pancreatic necrosis, skeletal muscle atrophy, and myonectin expression levels. Recombinant myonectin protein was administered in vivo and in vitro to assess its effects on acinar cell necrosis. Mechanistic insights were gained through RNA-seq data analysis and experimental validation. Serum samples from AP patients and healthy controls were collected to investigate the correlation between serum myonectin levels and disease severity.

Results The mouse model exhibited severe pancreatic necrosis, skeletal muscle atrophy, and elevated myonectin levels, with myonectin administration exacerbating model severity. We identified iron accumulation-induced ferroptosis as a key pathway contributing to myonectin-mediated acinar cell necrosis. A total of 22 healthy controls and 52 patients with varying degrees of AP were included in the serum samples and clinical data (36.5% females, age 49.79 ± 16.53). Analysis of serum samples revealed significantly higher myonectin levels in AP patients, correlating with disease severity ($R = 0.28$, $P = 0.041$).

Conclusions Our findings underscore the significant role of myonectin in SAP progression and its potential as a prognostic marker for disease severity in AP patients. This study contributes to a deeper understanding of the pathophysiology of SAP and highlights potential therapeutic targets for intervention.

†Xiaowu Dong, Weiwei Luo and Yaodong Wang contributed equally to this work.

*Correspondence:
Guotao Lu
pkulgt@163.com
Xiaolei Shi
092308@yzu.edu.cn
Jin Li
jinli807@126.com

Full list of author information is available at the end of the article

Keywords Severe acute pancreatitis, Skeletal muscle atrophy, Myonectin, Acinar cell necrosis, Organ crosstalk

Introduction

Severe acute pancreatitis (SAP) represents a critical progression from localized pancreatic injury to a systemic multisystem emergency, with approximately 20% of acute pancreatitis (AP) cases advancing to SAP. Despite advancements in treatment, SAP still carries a mortality rate ranging between 15% and 35% [1]. Notably, patients with SAP commonly exhibit weight loss and protein degradation [2], with over 50% experiencing persistent immune suppression and catabolic disorders [3–5], leading to skeletal muscle atrophy and increased mortality rates [3]. Moreover, retrospective analyses of domestic and international studies have underscored the association between skeletal muscle atrophy and the risk of pancreatitis [6, 7], with skeletal muscle atrophy identified as an independent risk factor for in-hospital SAP mortality [8]. However, gaps persist in our understanding of the metabolic changes occurring in skeletal muscles following AP and their potential contribution to pancreatic inflammation. Therefore, it is crucial to resolve these issues.

Skeletal muscle, the body's largest endocrine organ [9], secretes various myokines [10, 11], which have been extensively studied for their regulatory roles in physiological and metabolic pathways across diverse tissues and organs [12, 13]. Myokine secretion into the bloodstream could be possibly involved in the overall pathophysiological process of SAP [14]. Of particular interest is myonectin, a novel myokines implicated in regulating cellular iron metabolism and promoting iron accumulation within tissues and cells [15]. Intracellular iron accumulation, as facilitated by myonectin, precipitates the generation of oxygen free radicals via the Fenton reaction, which, in turn, instigates non-enzymatic lipid peroxidation and triggers cellular ferroptosis [16, 17]. Importantly, prior research, including our own, has indicated the pivotal role of ferroptosis in acinar cell necrosis [18, 19].

Building upon existing theories and prior research findings, the current study endeavors to establish an SAP mouse model through pancreatic duct ligation (PDL) to elucidate SAP complicated by skeletal muscle atrophy. Our objectives encompass observing the expression of myonectin in muscle tissue and serum, clarifying the mechanism by which exogenous myonectin exacerbates acinar cell necrosis through in vitro and in vivo experiments, and assessing the correlation between serum myonectin levels and disease severity in patients with clinical AP.

Materials and methods

Animals

C57BL/6 wild-type male mice (6–8 weeks, 20–23 g) were purchased from GemPharmatech Co. Ltd. (Nanjing, China). All mice were maintained in a specific pathogen-free (SPF) environment, provided with standard laboratory animal food and water, housed at a temperature of 23±2 °C, and subjected to a 12 h light-dark cycle.

Reagents and antibodies

Cholecystokinin (CCK8) was purchased from Echelon (471−47); Human Protein Myonectin ELISA Kit was purchased from CUSABIO (CSB-EL008059HU); LDH Cytotoxicity Assay Kit was purchased from Beyotime (C0017); Calcein-AM/PI Double Stain Kit and SYBR Green PCR Master Mix were acquired through YEASEN (40747ES, 11201ES); We purchased Amylase assay kit from BioSino(100000060) and Lipase assay kit from Nanjing Jiancheng Bioengineering (A054-1); FerroOrange was purchased from DOJINDO (F374); MDA Assay Kit was purchased from DOJINDO (M496); BODIPY 581/591 C11 was purchased from MedChemExpress (217075-36-0); We purchased anti-Myonectin and anti-GPX4 antibody from Abcam (ab125066, ab222468); Trizol was purchased from TIANGEN (DP424).

Construction of a severe acute pancreatitis model in mice pancreatic duct ligation and drug intervention

The SAP mouse model was constructed as previously reported [20]. C57BL/6J mice were anesthetized and placed on an operating table. An incision was made along the midline of the abdomen, exposing a small segment of the pancreatic duct, which was then ligated with 6−0 surgical suture and tied off. The abdomen was subsequently closed in layers. Recovery took place on a constant temperature heating pad at 37 °C for 60–90 min. Mice in the control group underwent laparotomy without duct ligation. Postoperatively, mice were provided with water and food, and changes in weight and survival rates were monitored daily. Tissue samples, including eye blood, pancreatic, and gastrocnemius muscle tissues, were collected from anesthetized mice on postoperative days 1, 2, 3, and 5. Tissues were handled with care to prevent damage.

C57BL/6J mice were randomly divided into five groups: sham surgery group, PDL model group, PDL+low-dose Myonectin (0.01ug/g), PDL+medium-dose Myonectin (0.1ug/g), and PDL+high-dose Myonectin (1ug/g), with 7 in each. Mice in the treatment groups received intraperitoneal injections of recombinant myonectin following recovery from PDL surgery. All mice were euthanized 60 h after PDL surgery, and pancreatic tissues were

collected. Blood samples were collected for enzymatic analyses.

Histopathology analysis

Pancreatic and muscle tissues were fixed and stained with hematoxylin-eosin (H&E). Observations and collection of representative images were conducted using a bright-field fluorescence microscope (BX53, Japan). Pathological tissue damage scores were independently evaluated by two pathologists. Pancreatic tissue damage was assessed based on tissue edema, inflammatory cell infiltration, and acinar cell necrosis [21]. Muscle tissue damage was identified by muscle cell shrinkage and increased intercellular space following muscle atrophy.

Amylase and lipase assay

Mouse retro-orbital venous blood samples were collected for amylase and lipase measurements. Blood samples were centrifuged (2000 rpm, 7 min) to obtain serum for appropriate dilution. The amylase and lipase levels were measured according to the manufacturer's instructions of the assay kits.

Western blot

10-20 mg gastrocnemius muscle tissues were weighed, followed by the addition of protein lysis buffer. Tissue proteins were extracted using a homogenizer and an ultrasonic machine, and stored at -20 °C. Protein samples were visualized using 12% SDS-PAGE and transferred to PVDF membrane. The filters were blocked with 5% skim milk at room temperature for 2 h, followed by incubation with primary antibodies at 4 °C for 12 h. Membranes were incubated with anti-rabbit immunoglobulin G at room temperature for 2 h followed by enhanced chemiluminescence reagent. The primary antibodies used for immunoblotting were anti-Myonectin (1:1000 dilution), anti-GPX4 (1:1000 dilution), and anti-GAPDH (1:500 dilution).

Nucleic acid detection

Open the nucleic acid analyzer, pipette 1ul ddH2O on the pedestal, click on blank, and pipette 1ul of sample on the pedestal. The A260/280nm wavelength was selected, the A260/280 ratio of pure RNA samples ranges from 1.8 to 2.0. The extracted RNA concentration range is from 0.1-5ug/ul. The RNA concentration and purity were measured and saved.

Quantitative real-time PCR analysis

10-20 mg gastrocnemius muscle tissues were weighed, and TRIzol reagent was added to extract total RNA. The RNA concentration and purity were measured, followed by cDNA synthesis using the RevertAid First Strand cDNA Synthesis Kit. The obtained cDNA was subjected to real-time qPCR using SYBR Green PCR Master Mix. The comparative CT (2^{-CT}) approach was used to measure the fold change of each mRNA, normalized to 18 S. The following primers were used:

18 S F: GGAAGTGCACCACCAGGAGT.
18 S R: TGCAGCCCCGGACATCTAAG.
MAFb-x F: CAGCTTCGTGAGCGACCTC.
MAFb-x R: GGCAGTCGAGAAGTCCAGTC.
MURF-1 F: GTGTGAGGTGCCTACTTGCTC.
MURF-1 R: GCTCAGTCTTCTGTCCTTGGA.

Isolation and treatment of pancreatic acinar cells (PACs)

Pancreatic tissue was isolated from C57BL/6 mice, and collagenase IV was used for tissue digestion and PAC separation [22]. After 17 min of digestion in a water bath, the digestion was terminated, followed by gentle blowing and sieving for centrifugation. Subsequently, cells were suspended in 2% FBS Hepes medium and incubated at 37 °C. Cellular injury was induced using 1 μm CCK, followed by exposure to gradually increasing concentrations of myonectin. After a 6-hour incubation, cells and supernatant were collected separately. LDH released into the supernatant was measured using an LDH cytotoxicity assay kit to assess the extent of PACs' death. Dual staining of PACs was performed using PI Solution and Calcein-AM Solution, followed by observation and imaging using a laser confocal microscope.

RNA-seq

RNA-seq data were obtained from the GEO database (GSE161945), including mRNA data from three SAP mouse samples and three control samples [23]. Differential analysis utilized the DESeq2 package, with genes selected based on an absolute log2FC value greater than or equal to 1 and a p-value of less than or equal to 0.05. Myonectin-related genes were filtered using the STRING database, identifying intersections with SAP differential genes. Enrichment analyses for KEGG and GO were performed for common genes.

Iron accumulation assay

Following the extraction and cultivation of PACs, they were stimulated with 1 μm CCK and 250 ng/ml Myonectin for 3 h. Subsequently, the cells were collected, washed twice with HBSS buffer, and subjected to staining by adding 1 umol of the Fe^{2+} detection probe FerroOrange, followed by an incubation at 37 °C for 30 min. The Fe^{2+} content inside the cells was observed using a laser confocal microscope. The fluorescence intensity was quantified using ImageJ software.

Lipid peroxidation levels assay

C11-BODIPY was employed to detect cellular lipid peroxidation levels. The methods used for PACs extraction,

cultivation, grouping, and drug treatment were the same as described above. Following a 3-hour drug stimulation of acinar cells, C11 was introduced, and the reaction ensued at 37 °C for 30 min. Subsequently, the cells were centrifuged to remove the supernatant and re-suspended in HBSS balanced salt solution. Utilizing appropriate excitation and emission wavelengths, a fluorescence plate reader was employed to analyze the content of lipid peroxidation products in the samples.

Moreover, 20–30 mg of pancreatic tissue samples were weighed, and lipid peroxidation levels in pancreatic tissues were measured in accordance with the instructions provided by the Malondialdehyde (MDA) Assay Kit. A fluorescence microplate reader was then used to detect the fluorescence intensity and calculate the MDA content in the samples.

Human subjects

Peripheral blood samples were collected from patients diagnosed with AP and admitted to the Affiliated People's Hospital of Yangzhou University from November 2021 to March 2023 for inclusion in the study.

The inclusion criteria were as follows: (1) age ranging from 18 to 85 years; (2) diagnosis meeting the 2012 revised Atlanta [24] AP diagnostic criteria; (3) onset time within 3 days; and (4) all patients were aware and signed informed consent forms. The exclusion criteria were as follows: (1) age < 18 or > 85 years; (2) symptom onset exceeding 3 days; (3) history of malnutrition, cachexia, myasthenia, chronic heart failure, chronic renal failure, or malignant tumors; and (4) pregnant women, individuals lacking decision-making capacity, and those with impaired behavioral abilities.

Basic demographic data, etiology, severity, changes in inflammatory factor levels, hospitalization duration, prognosis, CTSI score, and both local pancreatic and systemic complications were recorded.

Peripheral blood samples (3 mL) were collected from the patients, centrifuged at 3000 rpm for 7 min, and the upper serum layer was aspirated. Serum myonectin levels were determined using an ELISA kit, and the remaining samples were stored at -80 °C.

Statistical analyses

Continuous variables following a normal distribution are presented as mean ± standard deviation (mean ± SEM). T-tests or approximate t-tests were used for between-group comparisons based on variance homogeneity, while one-way ANOVA was used for multiple group comparisons. Non-normally distributed data were expressed as median (interquartile range) [M (P25, P75)], and group comparisons were conducted using the Mann-Whitney U test for two groups and the Kruskal-Wallis H test for multiple groups. Categorical variables were analyzed using the $\chi 2$ test, with Fisher's exact test employed when necessary. Pearson's correlation was used to explore the linear relationships between myonectin and various parameters including CTSI, WBC count, PCT, CRP, LDH, amylase, and hospitalization time. Statistical analyses were performed using R software (version 4.2.2), with significance set at $P < 0.05$.

Results

SAP model of pancreatic duct ligation in mice with skeletal muscle atrophy

PDL is a classical method used to induce SAP in mouse models (Fig. 1A). Post PDL surgery, the survival rates of mice decreased, with high mortality at 2–3 days (Fig. 1B). Ocular blood, pancreatic, and muscle tissues were collected on days 1, 2, 3, and 5 following PDL surgery. H&E staining revealed characteristic features of pancreatic damage in SAP mice, including inflammatory cell infiltration, acinar cell necrosis, and interstitial hemorrhage. Prolonged pancreatic duct obstruction exacerbated pancreatic necrosis, leading to severe morphological destruction. H&E staining of muscle tissue indicated muscle cell atrophy, enlarged myofiber gaps, and other typical signs of muscle atrophy (Fig. 1C). Furthermore, post PDL, mice experienced significant body weight loss of up to 30% (Fig. 1D). Skeletal muscle atrophy was further evaluated using qPCR to assess the expression of MuRF-1 (Muscle RING Finger 1) and MAFb-x (Muscle Atrophy F-box), revealing significant upregulation, particularly on days 1–2 post PDL (Fig. 1E-F), indicative of enhanced skeletal muscle protein degradation.

Significant increase in myonectin expression in SAP mouse model

Following the identification of signs of muscle atrophy in SAP mice, we assessed the expression of the myokine myonectin in circulation and tissues. Muscle tissue samples obtained at various time points underwent WB and qPCR analyses, demonstrating a significant increase in myonectin protein and mRNA levels starting from day 2 (Fig. 2A-C). ELISA was used to detect serum myonectin levels, revealing a significant increase in SAP mice (Fig. 2D). Under inflammatory stimuli, skeletal muscle status is altered, resulting in increased myonectin release, peaking in all parameters on day 2, coinciding with high mortality rates on days 2–3 in mice.

Myonectin aggravates acinar cell necrosis

This study used cholecystokinin (CCK) to establish a pancreatic acinar cell (PACs) injury model. Exogenous recombinant myonectin and a control solvent were administered and evaluated acinar cell death. We found that Myonectin significantly reduced lactate dehydrogenase (LDH) release (Fig. 3A). Moreover, fluorescence

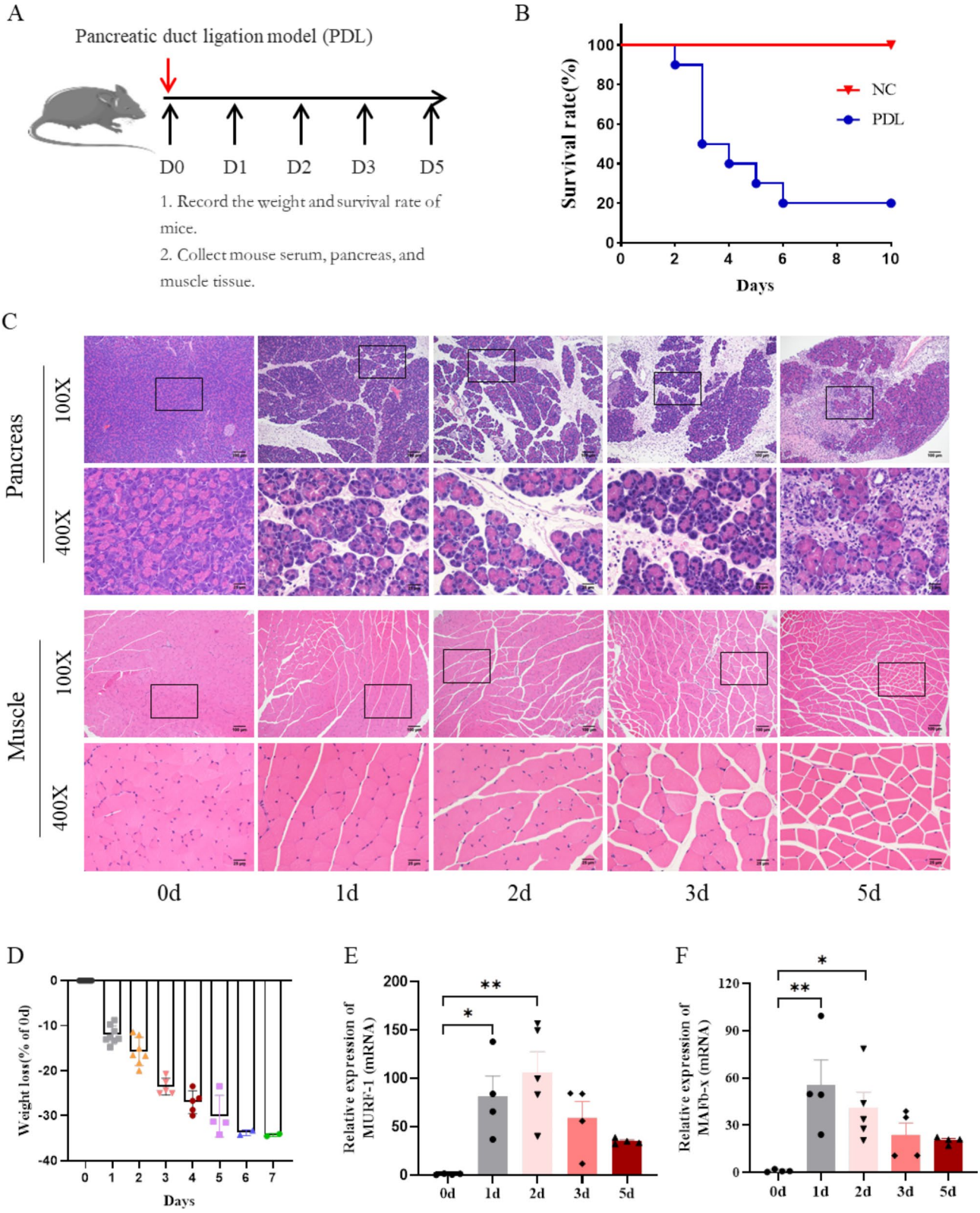

Fig. 1 Skeletal muscle atrophy observed in the SAP mouse model induced by pancreatic duct ligation (PDL). (**A**) Experimental protocol for establishing the SAP mouse model by PDL. (**B**) Survival rate of SAP mice. (**C**) Representative images of pancreatic and muscle tissue H&E staining in SAP mice. (**D**) Percentage of weight loss in SAP mice. (**E**, **F**) The mRNA levels of MURF-1 and MAFb-x in muscle tissues of SAP mice. $N \geq 4$, ns $p \geq 0.05$, * $p<0.05$, ** $p<0.01$, *** $p<0.001$

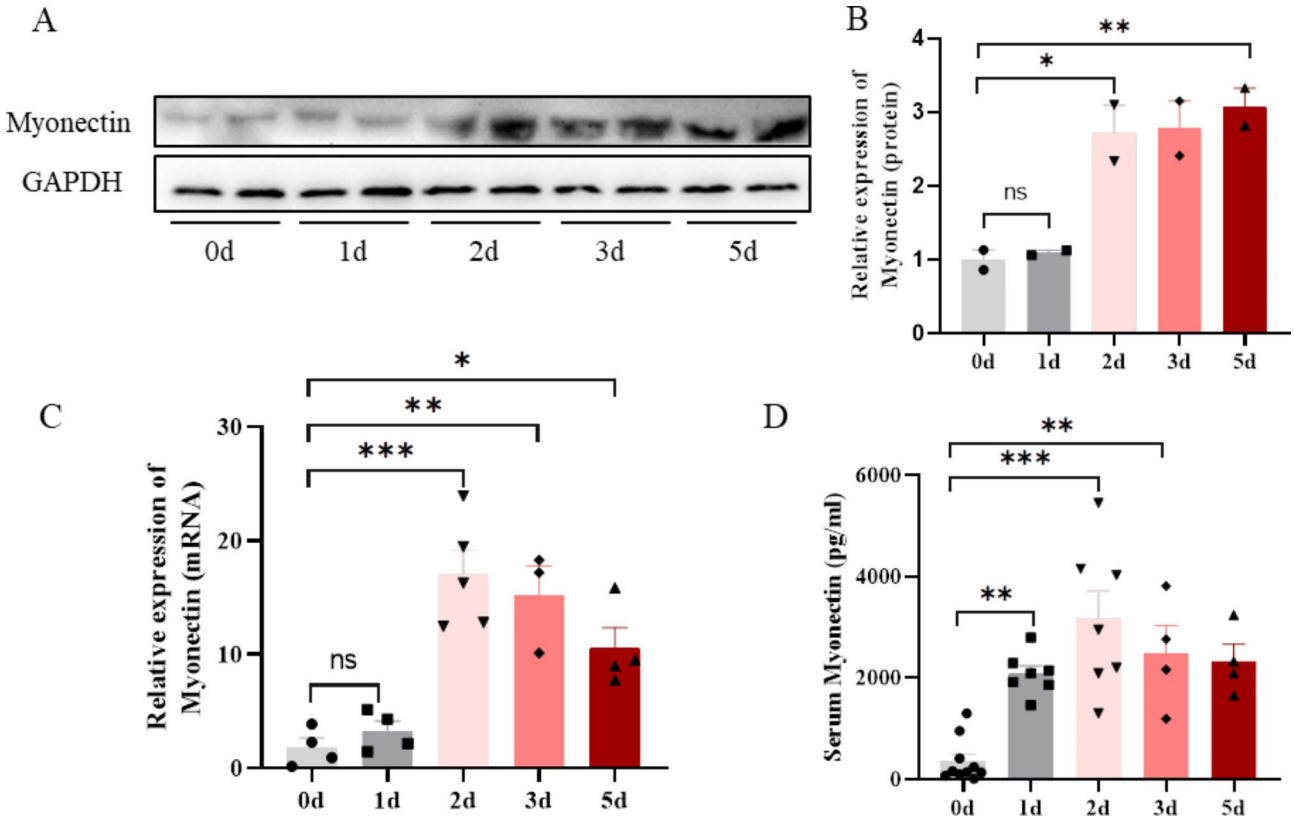

Fig. 2 Significant overexpression of the myokines myonectin in SAP mice. (**A**, **B**) Western blot and quantitative analysis of Myonectin in muscle tissue at different time points post PDL surgery. (**C**) qPCR detection of Myonectin in muscle tissue at different time points post PDL surgery. (**D**) ELISA detection of serum Myonectin levels in mice at different time points post PDL surgery. $N \geq 4$, ns $p \geq 0.05$, * $p<0.05$, ** $p<0.01$, *** $p<0.001$

double staining with calcein-AM/PI showed a significant increase in dead cells in the CCK+Myonectin treatment group compared to that in the CCK model group under confocal microscopy (Fig. 3B). Additionally, a dose-gradient experiment with the recombinant myonectin protein was conducted using the PDL model. We observed in PDL-induced experimental SAP model that exogenous myonectin significantly aggravated pancreatic histopathological damage, including pancreatic edema, inflammatory cell infiltration, and acinar cell necrosis (Fig. 3C-D). Serum levels of amylase and lipase were elevated (Fig. 3E-F). Both in vivo and in vitro experimental findings suggest that intervention with recombinant myonectin exacerbates acinar cell necrosis.

RNA-seq data identified pathways related to iron metabolism and ferroptosis as targets of myonectin

To explore the mechanism by which myonectin aggravates acinar cell necrosis, we screened the STRING database to identify myonectin-related genes (Fig. 4A), and intersected them with the SAP transcriptome database (GSE161945) to identify overlapping differentially expressed genes (Fig. 4B). Subsequently, KEGG and GO analyses were conducted on the shared genes, revealing significant alterations in iron metabolism pathways (Fig. 4C-D).

Myonectin increased iron accumulation in acinar cells and aggravated cell ferroptosis

In the CCK-induced PACs injury model, cells were incubated with recombinant myonectin protein. After 3 h of incubation, the Fe^{2+} detection probe FerroOrange was added, and fluorescence intensity was significantly higher in the CCK+Myonectin treatment group than in the CCK control group under laser confocal microscopy (Fig. 5A). WB analysis was performed to assess the expression levels of the ferroptosis key inhibitory protein glutathione peroxidase 4 (GPX4) in PACs, revealing lower GPX4 expression in CCK-induced cell damage following Myonectin treatment (Fig. 5B). Analysis of C11-BODIPY levels in acinar cells and MDA in pancreatic tissue showed a corresponding change in the degree of acinar cell lipid peroxidation following myonectin intervention. These findings indicate that iron accumulation-mediated ferroptosis is a key pathway by which myonectin aggravates acinar cell necrosis.

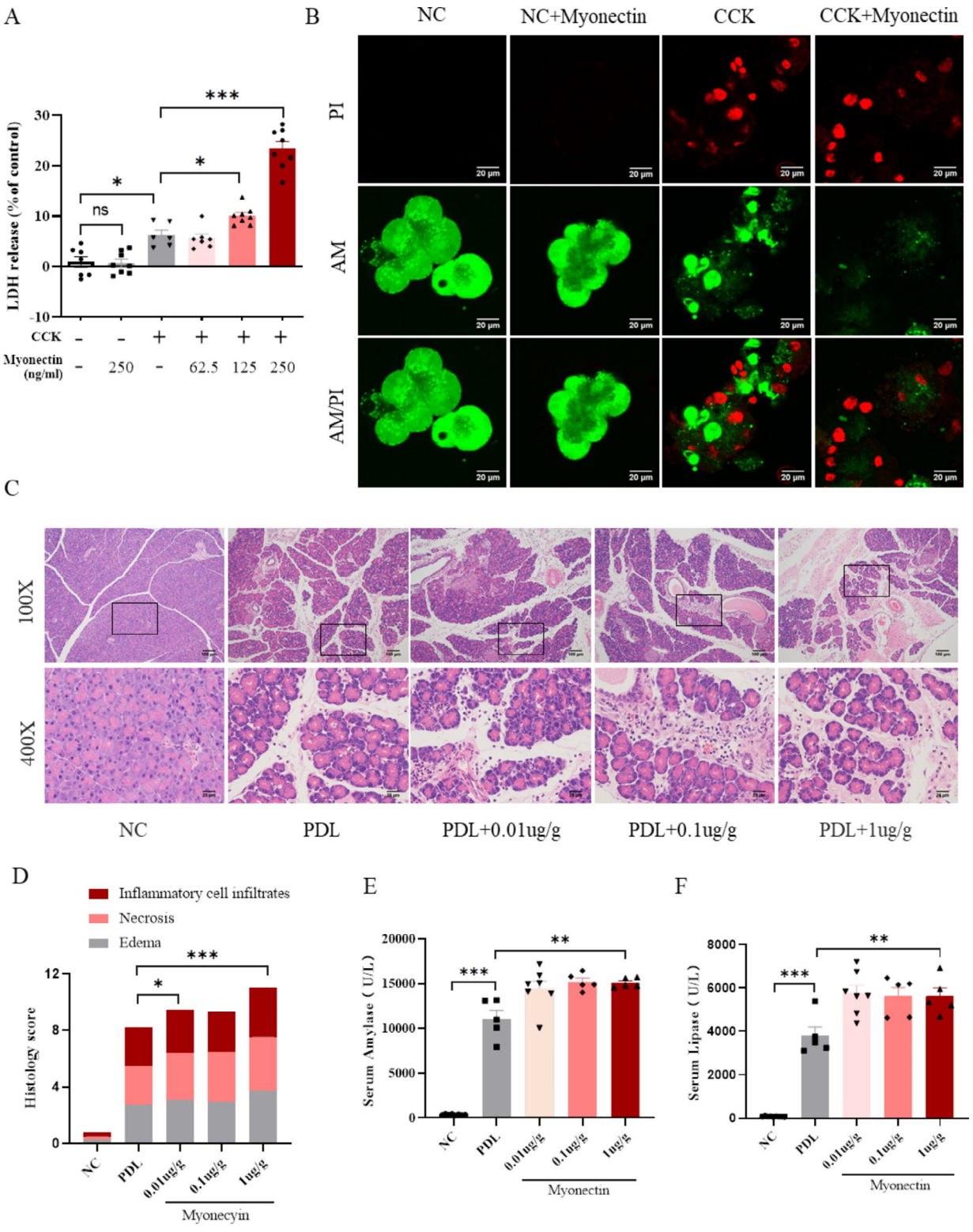

Fig. 3 Exogenous administration of recombinant myonectin protein aggravates acinar cell necrosis. (**A**) PACs were treated with CCK, together with gradient doses of Myonectin for 6 h; the levels of LDH release are shown. (**B**) Immunofluorescence imaging of pancreatic acinar cells stained with Calcein-AM/PI (1200x). (**C**) Representative images of pancreatic tissue H&E staining in PDL mice after treatment with gradient doses of recombinant Myonectin protein. (**D**) Pathological scoring of pancreatic tissue (edema, necrosis, inflammatory cell infiltration). (**E**) Serum amylase levels. (**F**) Serum lipase levels. CCK, cholecystokinin; AM, acetoxymethyl, represents living cells; PI, propidium iodide, represents dead cells. $N \geq 5$, ns $p \geq 0.05$, * $p<0.05$, ** $p<0.01$, *** $p<0.001$

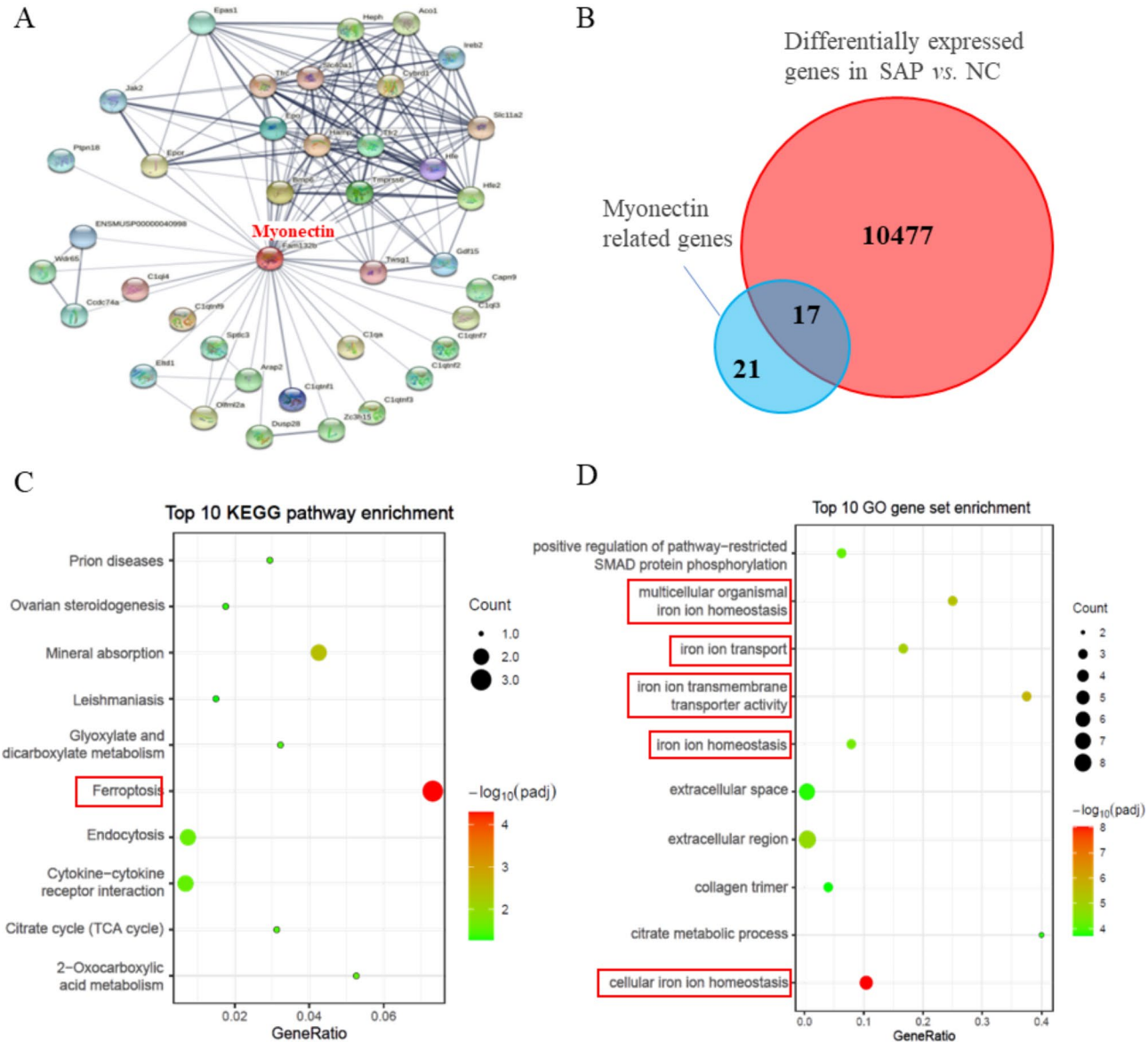

Fig. 4 RNA-seq data identified pathways related to iron metabolism and ferroptosis as targets of myonectin. (**A**) Myonectin related genes were screened in the String database. (**B**) Overlap of myonectin-related genes from the String database with RNA-seq data in the SAP model identified 17 common genes. (**C**) KEGG enrichment analysis of these 17 genes. (**D**) GO enrichment analysis of these 17 genes

Evaluation of serum myonectin levels in healthy participants and patients with AP

A total of 74 participants were included in the study. The study design flowchart is shown in Fig. 6A. AP was further categorized as mild (MAP, $n=21$), moderately severe (MSAP, $n=20$), or severe (SAP, $n=11$). Clinical data, including general clinical and demographic data of patients with AP, are shown in Table 1.

Serum myonectin levels revealed a correlation between myonectin levels and disease severity (Fig. 6B). It appears that with increased myonectin there is an increase in disease severity. Significant differences in serum myonectin levels were observed between patients with and without acute necrotic tissue accumulation ($P<0.01$); however, no correlation was observed with organ failure (Fig. 6C). Further correlation analysis revealed a linear relationship between serum Myonectin levels and CTSI (Computed Tomography Severity Index) for AP ($R=0.28$, $P=0.041$) (Fig. 6D). Additionally, serum myonectin levels showed significant associations with WBC count, CRP level, LDH level, and hospitalization time (Fig. 6E).

Discussion

In this study, we demonstrated that mice with SAP exhibit typical skeletal muscle atrophy, leading to an increase in myonectin secretion. Myonectin aggravates

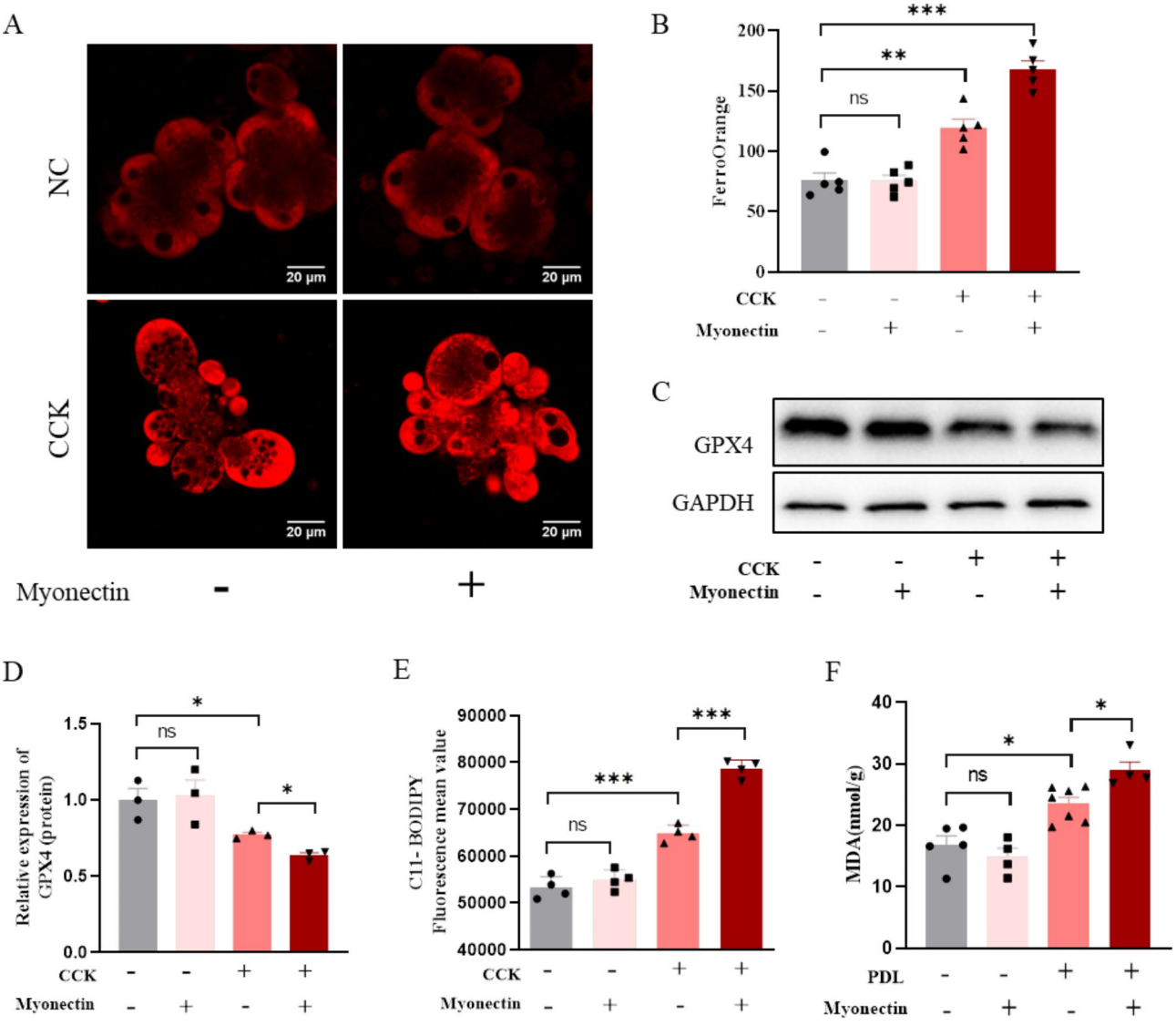

Fig. 5 Myonectin induced iron accumulation and intensified acinar cell ferroptosis. (**A**) Immunofluorescence imaging of pancreatic acinar cells stained with FerroOrange (1200x). (**B**) Quantitative analysis of fluorescence intensity ($N \geq 5$). (**C**) Western blot detection of key ferroptosis protein GPX4 expression levels in PACs. (**D**) Quantitative analysis of GPX4 expression changes. (**E**) C11-BODIPY measurement of cellular lipid peroxidation levels. (**F**) MDA assessment of lipid peroxidation levels in pancreatic tissue. $N \geq 4$, ns $p \geq 0.05$, * $p<0.05$, ** $p<0.01$, *** $p<0.001$

acinar cell ferroptosis via iron accumulation, thus worsening pancreatic injury in SAP. Clinically, we proposed, for the first time, a correlation between serum myonectin levels in patients with AP and the clinical severity and prognosis.

Severe acute pancreatitis is a perilous condition characterized by rapid disease progression and an increased risk of mortality. Among patients with SAP, 69.6% exhibit skeletal muscle atrophy, with only 28.8% able to return to work, leading to poor long-term quality of life [3]. Currently, the primary methods for establishing SAP mouse models include retrograde biliopancreatic duct injection, PDL, and caerulein injection [25–27]. To mitigate the influence of exogenous drugs on the natural course of SAP, we used a PDL surgical model. Our team conducted numerous experiments to investigate this model [20, 28].

Inflammation and various other stimuli trigger increased myokine secretion, which can induce muscle dysfunction through autocrine or paracrine signaling and, conversely, exacerbate inflammation through endocrine pathways [29]. This potentially establishes a vicious cycle that perpetuates SAP and skeletal muscle atrophy. We found significant upregulation of myonectin during the progression of SAP, leading to its release into the peripheral circulation. Intervention with exogenous myonectin recombinant protein aggravates acinar cell damage and pancreatic tissue necrosis. Our study indicates an organ dialogue between the pancreas and muscles,

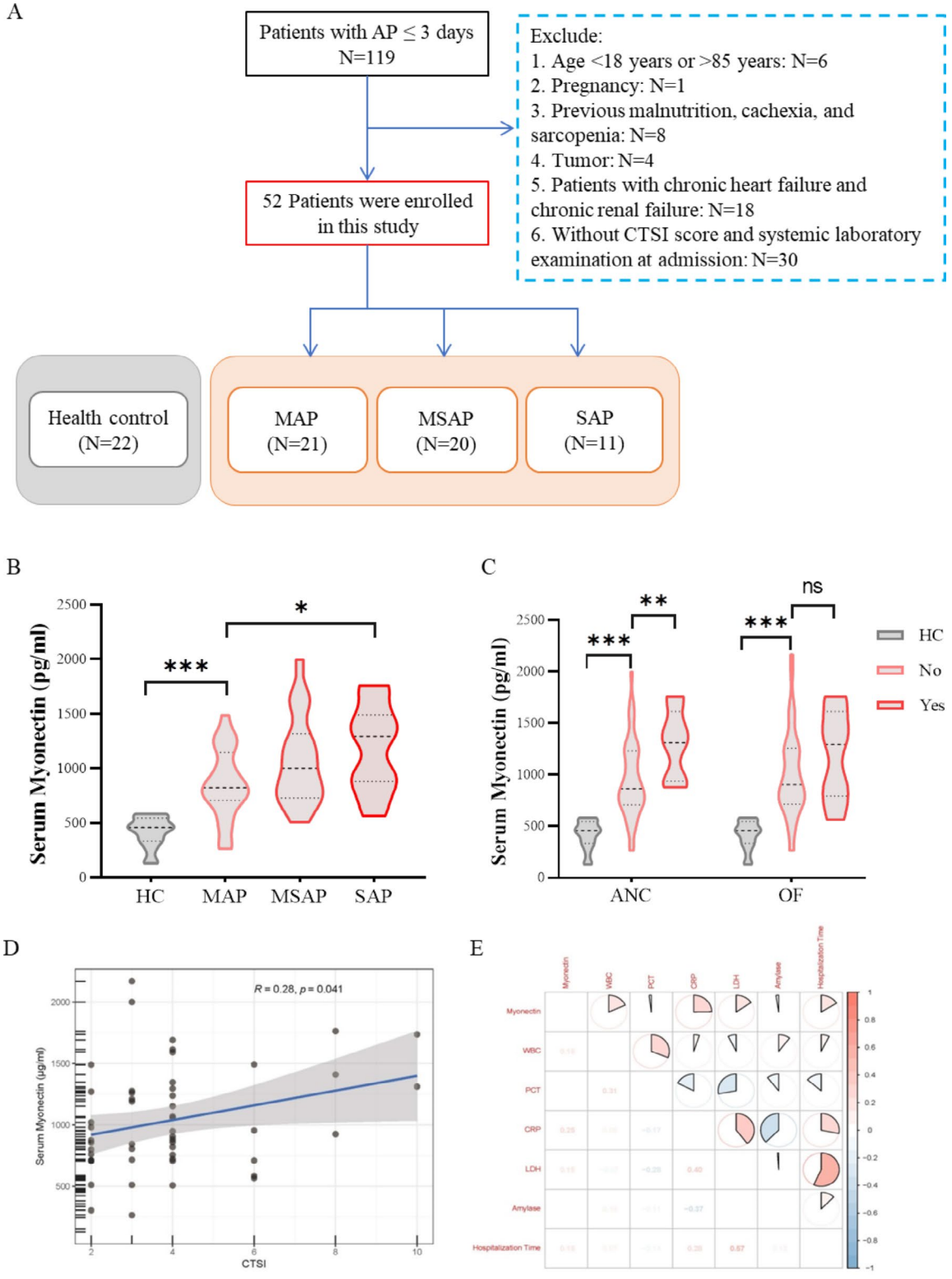

Fig. 6 Serum myonectin levels were correlated with the severity and pancreatic necrosis of AP patients. (**A**) Flowchart of the patients with AP in the clinical study. (**B**) ELISA analysis of serum Myonectin levels in the healthy control group and different severity levels of AP patients. (**C**) Correlation analysis of patient serum Myonectin with ANC and OF. (**D**) Correlation analysis of patient serum Myonectin with CTSI. (**E**) Correlation coefficient heat map of serum Myonectin levels upon admission with other clinical parameters. ns $p \geq 0.05$, * $p<0.05$, ** $p<0.01$, *** $p<0.001$. HC, health check; MAP, mild AP; MSAP, moderately severe AP; SAP, severe AP; ANC, absolute neutrophil count; OF, organ failure; CTSI, CT severity index; WBC, white blood cells; PCT, procalcitonin; CRP, C-reactive protein; HCT, hematocrit; LDH, lactate dehydrogenase

Table 1 Baseline characteristics of AP patients

Characteristics	Total (n = 52)	MAP (n = 21)	MSAP (n = 20)	SAP (n = 11)	p
Sex(Male)	33 (63.46)	13 (61.90)	14 (70)	6 (54.55)	0.660
Age	49.79 ± 16.53	50 ± 16.20	48.20 ± 16.38	52.27 ± 18.63	0.810
BMI	24.57 (22.73, 26.40)	23.44 (22.20, 26.30)	24.93 (23.30, 26.74)	24.8 (23.26, 26.16)	0.542
Etiology					0.349
BAP	21 (40.38)	8 (38.10)	10 (50)	3 (27.27)	
HLAP	24 (46.15)	8 (38.10)	9 (45)	7 (63.64)	
Other	7 (13.46)	5 (23.81)	1 (5)	1 (9.09)	
APFC	36 (69.23)	8 (38.10)	17 (85)	11 (100)	< 0.001
PPC	4 (7.69)	0	1 (5)	3 (27.27)	0.013
ANC	7 (13.46)	0	0	7 (63.64)	< 0.001
WON	1 (1.92)	0	0	1 (9.09)	0.212
OF	9 (17.31)	0	0	9 (81.82)	< 0.001
ARDS	8 (15.38)	0	0	8 (72.73)	< 0.001
Shock	3 (5.77)	0	0	3 (27.27)	0.007
AKI	3 (5.77)	0	0	3 (27.27)	0.007
CTSI	4 (2.75, 4)	2 (2, 3)	4 (4, 4)	6 (6, 8)	< 0.001
WBC	12.47 ± 3.93	11.35 ± 4.06	13.71 ± 4.17	12.36 ± 2.66	0.159
PCT	0.21 ± 0.08	0.20 ± 0.06	0.22 ± 0.07	0.22 ± 0.12	0.809
CRP	105.35 (18.82, 203.83)	37.59 (13.80, 99.86)	161.97 (75.17, 223.61)	164.51 (108.68, 293.07)	0.009
LDH	287.15 (220.27, 393)	223.1 (205, 274)	313.50 (247.50, 361.75)	790 (449, 1332)	< 0.001
Amylase	365 (149.50, 680)	475 (177, 1319.75)	293 (133, 553.50)	555 (213.50, 812.50)	0.290
Hospitaly time	10.50 (7.75, 15)	9 (5, 11)	10 (8.50, 12.25)	20 (17, 29)	< 0.001

MAP, mild AP; MSAP, moderately severe AP; SAP, severe AP; BMI, body Mass Index; BAP, biliary acute pancreatitis; HLAP, hyperlipidemic acute pancreatitis; APFC, acute peripancreatic fluid; PPC, pancreatic pseudocyst; ANC, absolute neutrophil count; WON, walled-off necrosis; OF, organ failure; ARDS, acute respiratory distress syndrom; AKI, acute kidney injury; CTSI, CT Severity Index; WBC, white blood cells; PCT, procalcitonin; CRP, C-reactive protein; LDH, lactate dehydrogenase

in which myonectin plays an important role. Research on death pathways in pancreatic necrosis and treatment targets has been a focal point in basic research [30, 31]. Previous studies demonstrated the downregulation of GPX4 mRNA and protein levels in pancreatic tissue in an AP animal model [18, 19], suggesting ferroptosis as a critical mode of acinar cell death. FerroOrange, a novel fluorescent probe, reflects intracellular Fe^{2+} accumulation during ferroptosis, when the membrane repair enzyme GPX4 becomes dysfunctional, leading to the accumulation of oxygen radicals [32]. C11, a fluorescent probe used to measure lipid peroxidation, is localized on the active cell membrane. MDA, a secondary product of lipid peroxidation, is commonly used as an indicator in cells and tissues [33]. Our findings indicate significant changes in ferroptosis markers in the SAP model following exogenous myonectin administration, elucidating the specific pathway by which myonectin aggravates acinar cell necrosis through iron accumulation.

The expression of serum myonectin and its association with clinical severity in patients with AP remain unreported. This study marks the first investigation into serum myonectin levels in patients with AP of varying severity and their integration with clinical data. The treatment focus in the early stages of SAP primarily addresses organ failure, shifting to managing complications such as infected necrotic tissue accumulation during later stages [34]. We observed significant differences in serum myonectin levels among patients grouped according to the presence or absence of acute necrotic tissue accumulation, indicating a relationship with pancreatic acinar cell damage, rather than a systemic inflammatory response. Early assessment of the severity of AP is crucial for the detection and prompt treatment of severe cases [35]. CTSI is a fundamental indicator for assessing the extent of local inflammation and necrosis in AP [36]. The linear correlation between serum myonectin levels and CTSI further suggests that myonectin exacerbates local pancreatic damage. Furthermore, there is a correlation between myonectin levels and disease severity in patients with AP. In the future, myonectin may serve as a prognostic marker for the clinical management of AP.

Limitations of the study

Our study lacked data on skeletal muscle atrophy in patients with AP. However, in the field of imaging, numerous reports have measured the skeletal muscle area of AP patients [37, 38], and it is generally believed that SAP is associated with skeletal muscle atrophy accompanied by cachexia. Furthermore, clinical samples were obtained from a single-center source, and the sample size was small.

Conclusion

Our study focused on the interaction between SAP and skeletal muscle atrophy. We initially confirmed that the myokine myonectin induces iron accumulation, exacerbating acinar cell ferroptosis, with a correlation between serum myonectin levels in patients with AP and disease severity. Furthermore, exploring therapeutic interventions targeting myonectin or investigating other potential mediators of skeletal muscle and pancreatic interactions, would provide direction for subsequent studies in the field.

Acknowledgements
We want to express our gratitude and respect to the patients who have joined the group.

Author contributions
XLS, WJG and GTL contributed to study design. XWD and WWL performed experiments; YDW and QTZ contributed to clinical data analysis. WWL and YDW contributed to manuscript writing. XWD, XLS, WMX, GTL and JL contributed to funding acquisition. All authors read and approved the final manuscript.

Funding
This work was supported by the National Natural Science Foundation of China (no. 82200996, 82270680 and 82200720), Yangzhou Key Research and Development Program (Social Development) Project (no. YZ2022080), Natural Science Research of Jiangsu Higher Education Institutions of China (no. 22KJB320028), Special Fund for Science and Technology Innovation Teams of Shanxi Province (No. 202304051001021), Shanxi Funding for High Level Overseas Returns (2022).

Data availability
No datasets were generated or analysed during the current study.

Declarations

Ethics approval and consent to participate
The animal study protocol was approved by the Ethics Committee of Yangzhou University (Approval No. 202202127). The clinical biospecimen repository has received approval from the Clinical Ethics Committee of the Affiliated Hospital of Yangzhou University (Approval No. 2018-YKL11-27). Informed consent has been obtained for collecting all the samples.

Consent for publication
Not applicable.

Competing interests
The authors declare no competing interests.

Author details
[1]Pancreatic Center, Department of Gastroenterology, The Affiliated Hospital of Yangzhou University, Yangzhou University, Yangzhou, Jiangsu, China
[2]Department of Gastroenterology, Kunshan Hospital of Traditional Chinese Medicine, Affiliated Hospital of Yangzhou University, Kunshan, Jiangsu, China
[3]Laboratory of Intensive Care of Yangzhou, The Affiliated Hospital of Yangzhou University, Yangzhou University, Yangzhou, Jiangsu, China
[4]Department of Endocrinology and Metabolism, The Second Hospital of Shanxi Medical University, Shanxi Medical University, 56 Xin Jian Road, Tai Yuan, Shan Xi, China

Received: 22 July 2024 / Accepted: 24 November 2024
Published online: 03 December 2024

References

1. Ingraham NE, King S, Proper J, Siegel L, Zolfaghari EJ, Murray TA, et al. Morbidity and mortality trends of Pancreatitis: an observational study. Surg Infect (Larchmt). 2021;22:1021–30.
2. Rysgaard S, Rasmussen D, Novovic S, Schmidt PN, Gluud LL. Effect of overweight and obesity on weight loss and length of stay in patients with walled-off pancreatic necrosis. Nutrition. 2017;38:109–12.
3. Yang N, Li B, Ye B, Ke L, Chen F, Lu G, et al. The long-term quality of life in patients with persistent inflammation-immunosuppression and catabolism syndrome after severe acute pancreatitis: a retrospective cohort study. J Crit Care. 2017;42:101–6.
4. Hawkins RB, Raymond SL, Stortz JA, Horiguchi H, Brakenridge SC, Gardner A, et al. Chronic critical illness and the persistent inflammation, immunosuppression, and catabolism syndrome. Front Immunol. 2018;9:1511.
5. Gentile LF, Cuenca AG, Efron PA, Ang D, Bihorac A, McKinley BA, et al. Persistent inflammation and immunosuppression: a common syndrome and new horizon for surgical intensive care. J Trauma Acute Care Surg. 2012;72:1491–501.
6. Sternby H, Mahle M, Linder N, Erichson-Kirst L, Verdonk RC, Dimova A, et al. Mean muscle attenuation correlates with severe acute pancreatitis unlike visceral adipose tissue and subcutaneous adipose tissue. United Eur Gastroenterol J. 2019;7:1312–20.
7. Zhou Y, Hao N, Duan Z, Kong M, Xu M, Zhang D, et al. Assessment of Acute Pancreatitis Severity and Prognosis with CT-Measured body composition. Int J Gen Med. 2021;14:3971–80.
8. van Grinsven J, van Vugt JLA, Gharbharan A, Bollen TL, Besselink MG, van Santvoort HC, et al. The Association of Computed Tomography-Assessed Body Composition with mortality in patients with necrotizing pancreatitis. J Gastrointest Surg. 2017;21:1000–8.
9. Iizuka K, Machida T, Hirafuji M. Skeletal muscle is an endocrine organ. J Pharmacol Sci. 2014;125:125–31.
10. Pedersen L, Hojman P. Muscle-to-organ cross talk mediated by myokines. Adipocyte. 2012;1:164–7.
11. Chen W, Wang L, You W, Shan T. Myokines mediate the cross talk between skeletal muscle and other organs. J Cell Physiol. 2021;236:2393–412.
12. Gomarasca M, Banfi G, Lombardi G, Myokines. The endocrine coupling of skeletal muscle and bone. Adv Clin Chem. 2020;94:155–218.
13. Das DK, Graham ZA, Cardozo CP. Myokines in skeletal muscle physiology and metabolism: recent advances and future perspectives. Acta Physiol (Oxf). 2020;228:e13367.
14. Petrov MS. Skeletal muscle: a new piece in the pancreatitis puzzle. United Eur Gastroenterol J. 2019;7:1283–4.
15. Srole DN, Ganz T. Erythroferrone structure, function, and physiology: Iron homeostasis and beyond. J Cell Physiol. 2021;236:4888–901.
16. Latunde-Dada GO, Ferroptosis. Role of lipid peroxidation, iron and ferritinophagy. Biochim Biophys Acta Gen Subj. 2017;1861:1893–900.
17. Hirschhorn T, Stockwell BR. The development of the concept of ferroptosis. Free Radic Biol Med. 2019;133:130–43.
18. Ma X, Dong X, Xu Y, Ma N, Wei M, Xie X et al. Identification of AP-1 as a critical Regulator of glutathione peroxidase 4 (GPX4) transcriptional suppression and Acinar Cell Ferroptosis in Acute Pancreatitis. Antioxid (Basel). 2022;12.
19. Luo W, Chen L, Sun H, Zhang S, Dong X, Pan J et al. Soat2 inhibitor avasimibe alleviates acute pancreatitis by suppressing acinar cell ferroptosis. Naunyn Schmiedebergs Arch Pharmacol. 2024.
20. Han F, Ding ZF, Shi XL, Zhu QT, Shen QH, Xu XM, et al. Irisin inhibits neutrophil extracellular traps formation and protects against acute pancreatitis in mice. Redox Biol. 2023;64:102787.
21. Yuan C, Dong X, Xu S, Zhu Q, Xu X, Zhang J, et al. AKBA alleviates experimental pancreatitis by inhibiting oxidative stress in macrophages through the Nrf2/HO-1 pathway. Int Immunopharmacol. 2023;121:110501.
22. Zhu Q, Yuan C, Dong X, Wang Y, Li B, Tu B et al. Bile acid metabolomics identifies chenodeoxycholic acid as a therapeutic agent for pancreatic necrosis. Cell Rep Med. 2023;101304.
23. Wang B, Wu J, Huang Q, Yuan X, Yang Y, Jiang W, et al. Comprehensive Analysis of differentially expressed lncRNA, circRNA and mRNA and their ceRNA networks in mice with severe Acute Pancreatitis. Front Genet. 2021;12:625846.
24. Banks PA, Bollen TL, Dervenis C, Gooszen HG, Johnson CD, Sarr MG, et al. Classification of acute pancreatitis–2012: revision of the Atlanta classification and definitions by international consensus. Gut. 2013;62:102–11.
25. Zhu CJ, Yang WG, Li DJ, Song YD, Chen SY, Wang QF, et al. Calycosin attenuates severe acute pancreatitis-associated acute lung injury by curtailing

high mobility group box 1 - induced inflammation. World J Gastroenterol. 2021;27:7669–86.
26. Lin T, Song J, Pan X, Wan Y, Wu Z, Lv S, et al. Downregulating Gasdermin D reduces severe Acute Pancreatitis Associated with Pyroptosis. Med Sci Monit. 2021;27:e927968.
27. Glaubitz J, Wilden A, Frost F, Ameling S, Homuth G, Mazloum H, et al. Activated regulatory T-cells promote duodenal bacterial translocation into necrotic areas in severe acute pancreatitis. Gut. 2023;72:1355–69.
28. Wu Z, Lu G, Zhang L, Ke L, Yuan C, Ma N, et al. Protectin D1 decreases pancreatitis severity in mice by inhibiting neutrophil extracellular trap formation. Int Immunopharmacol. 2021;94:107486.
29. Kalinkovich A, Livshits G. Sarcopenic obesity or obese sarcopenia: a cross talk between age-associated adipose tissue and skeletal muscle inflammation as a main mechanism of the pathogenesis. Ageing Res Rev. 2017;35:200–21.
30. Lee PJ, Papachristou GI. New insights into acute pancreatitis. Nat Rev Gastroenterol Hepatol. 2019;16:479–96.
31. Ma N, Yuan C, Shi J, Zhu Q, Liu Y, Ma X et al. Interleukin-37 protects against acinar cell pyroptosis in acute pancreatitis. JCI Insight. 2022;7.
32. Yang WS, SriRamaratnam R, Welsch ME, Shimada K, Skouta R, Viswanathan VS, et al. Regulation of ferroptotic cancer cell death by GPX4. Cell. 2014;156:317–31.
33. Tsikas D. Assessment of lipid peroxidation by measuring malondialdehyde (MDA) and relatives in biological samples: Analytical and biological challenges. Anal Biochem. 2017;524:13–30.
34. Zhou HJ, Mei X, He XH, Lan TF, Guo SB. Severity stratification and prognostic prediction of patients with acute pancreatitis at early phase a retrospective study. Medicine. 2019;98.
35. Fung C, Svystun O, Fouladi DF, Kawamoto S. CT imaging, classification, and complications of acute pancreatitis. Abdom Radiol. 2020;45:1243–52.
36. Alberti P, Pando E, Mata R, Vidal L, Roson N, Mast R, et al. Evaluation of the modified computed tomography severity index (MCTSI) and computed tomography severity index (CTSI) in predicting severity and clinical outcomes in acute pancreatitis. J Digest Dis. 2021;22:41–8.
37. Jalal M, Rosendahl J, Campbell JA, Vinayagam R, Al-Mukhtar A, Hopper AD. Identification of Digital Sarcopenia Can Aid the Detection of Pancreatic Exocrine Insufficiency and Malnutrition Assessment in patients with suspected pancreatic Pathology. Digest Dis. 2022;40:335–44.
38. Akturk Y, Gunes SO, Hekimoglu B. The effects of the Fat distribution of body, skeletal muscle Mass and muscle quality on Acute Pancreatitis Severity: a retrospective cross-sectional study. J Comput Assist Tomo. 2021;45:500–6.

Publisher's note